INTERNATIONAL JOURNAL OF HYDROGEN ENERGY 40 (2015) 16775–16785

Available online at www.sciencedirect.com

ScienceDirect

journal homepage: www.elsevier.com/locate/he

Thermal conductivity in the three layered regions of micro porous layer coated porous transport layers for the PEM fuel cell

Odne S. Burheim [a,*,1], Gregory A. Crymble [b,1], Robert Bock [a,c,2], Nabeel Hussain [b,2], Sivakumar Pasupathi [d,2], Anton du Plessis [e,2], Stephan le Roux [e,2], Frode Seland [c,2], Huaneng Su [d,2], Bruno G. Pollet [d,f]

[a] Department of Electrical and Computational Engineering, HiST – Sor-Trondelag University College, Trondheim, Norway

[b] Department of Chemical Engineering, University of Cape Town, South Africa

[c] Department of Materials Science and Technology, Norwegian University of Science and Technology, 7491 Trondheim, Norway

[d] South African Institute for Advanced Materials Chemistry (SAIAMC), Faculty of Natural Sciences, University of the Western Cape, Cape Town, South Africa

[e] University of Stellenbosch, Private Bag X1, Matieland, Stellenbosch, South Africa

[f] Eau2Energy, Nottingham, NG14 6DX, England, UK

ARTICLE INFO

Article history:
Received 27 March 2015
Received in revised form
30 July 2015
Accepted 31 July 2015
Available online 8 September 2015

Keywords:
Polymer electrolyte membrane fuel cell
Thermal conductivity
Micro porous layer
Gas diffusion layer
Computer tomography

ABSTRACT

Thermal conductivity of the polymer electrolyte membrane fuel cell (PEMFC) components has achieved increased attention over the past decade. Despite the fact that the PEMFC itself (between the gas flow plates) is less than a millimetre in thickness, several °C temperature differences can arise inside it during operation. These temperature differences mainly arise across the porous transport layers (PTL) often also referred to as gas diffusion layers (GDL). Several research efforts have led to a good understanding of the thermal conductivity of the PTL; in particular to how this property changes with compression, temperature, PTFE content, different fabrics, and water content. Far less attention has been given to the thermal conductivity of the much thinner layered micro porous layer (MPL) and in particular to the thermal conductivity of the transitional region between the PTL and the MPL.

In this study we have used X-ray computer tomography (XCT), scanning electron microscopy (SEM), and thermal conductivity measurements to show that a MPL coated PTL is actually a three layered structure where the PTL is on one side, the MPL on the other, and a composite region consisting of the MPL as a matrix with the PTL fibres in the middle. We have shown that the thermal conductivity of the MPL-PTL-composite region is much larger than for the two others and that temperature differences inside this layer can be neglected compared to the regions where it is MPL-only and PTL-only. We have

* Corresponding author.
E-mail address: odnesb@hist.no (O.S. Burheim).
[1] Authors share equal contributions to the manuscript.
[2] Listed alphabetically.

http://dx.doi.org/10.1016/j.ijhydene.2015.07.169

also shown that the MPL has a significantly lower thermal conductivity than the other two layers. In light of this research, the MPL of the commercial SGL should be integrated into the GDL in order to have lower temperature deviations in the PEMFC. A relevant literature review is included.

Introduction

Hydrogen can be extracted from a wide range of renewable and non-renewable sources and is the chemically bound fuel with the highest available gravimetric energy density. The low temperature PEMFC is currently one of the most promising tools for converting the chemically bound energy directly into electric energy for the automotive industry, in part due to the simple and flexible start-up and shut-down and also because of the efficient systems developed over the past decades. Next to catalyst developments (cost) and ageing (durability and degradation), thermal management and engineering constitute an important aspect of component and systems engineering now and in the future [1–3]. This paper presents an overview of the efforts in determining component through-plane thermal conductivity relevant for stationary PEMFC operation with a particular focus on the micro porous layer (MPL) and its bridge with the porous transport layer (PTL), also referred to as the gas diffusion layer (GDL).

The role of the MPL

The PEMFC is typically symmetrical and consists of a catalyst layer (CL), a MPL and a porous transport layer (PTL) situated on each side of a membrane, with the entire assembly enclosed by polarisation plates. The polarisation plates have channels for gas flow and water removal engraved into them. The water typically stems from the reaction in the cathode catalyst layer. From there it must pass through the MPL and the PTL in order to get to the gas flow channels. The micro porous layer (MPL) has been used to improve the performance of the PEMFC for more than a decade. Initially it was used to make a support for the CL [4] though it has also been shown that it is extremely important for water management. In addition to supporting the CL, the MPL aids water removal thus improving the mass transport of the feed gases (oxygen and hydrogen) to the CL.

Several studies have dealt with how the MPL affects the water transport. Qi and Kaufmann demonstrated that the MPL is important to avoid flooding and that once an MPL is present, the backing material itself is not really that important (however, this may not be the case when it comes to thermal conductivity of course) [5]. Gostick et al. studied liquid water breakthrough at the cathode side by measuring water saturation and capillary pressure on PTLs in the gas channel with and without a MPL [6]. They found that the PTL saturation at the point of water breakthrough (water channelling through the PTL and reaching the gas channel) was reduced from 27% to less than 3% as a result of the MPL restricting the number of water pathways through the PTL. Lee et al. used synchrotron X-ray radiography to observe the through-plane liquid water distribution in an operating PEMFC with and without MPL [7]. They found that the MPL increases the number of breakthrough locations and suggest that this reduces the saturation level in the PTL and water agglomeration at the catalyst layer/MPL interface resulting in improved performance. Deevanhxay et al. used soft X-ray radiography to visualize liquid water accumulation in the MEA with and without MPL during operation [8]. They found that the liquid water accumulates in the PTL under the flow field land/rib both with and without MPL. The MPL was shown to act as a buffer between the CL and the accumulated liquid water in the PTL. Based on this result and polarization curve analysis, they conclude that the MPL improves performance by causing a reduction in water accumulation at the CL/PTL interface. Several other studies debate what other effects the MPL has for the water transport in the PEMFC and an overview is given elsewhere [9].

From the literature, it is clear that the MPL affects water management in a benign manner and that it supports the catalyst layer. It is less understood how the MPL actually affects local thermal conductivity and temperature profiles however. In this paper, we dedicate our effort to this point.

Thermal conductivity measurements of PEMFC porous layered components

Providing reliable measurements of the thermal conductivity of PEMFC components and materials is both important and challenging. Internationally, there are several groups that have looked into this task. The materials investigated range in thickness from around 20 μm up to 400 μm and some of them are so porous that they do not entirely cover their area, *i.e.* their porosity and thickness in combination results in several open areas or spots. In the studies of the thermal conductivity of these materials the compressibility, temperature, PTFE content, ageing mechanisms, and water content have been applied as parameters for the thermal conductivity, albeit the parameters were never all included in a single study. Depending on the material type and properties three approaches can be used to determine the thermal conductivity of the MPL, *i.e.* the *ex-situ* compressible flux meter method, the *in-situ* temperature sensor method, and the laser flash method. In this brief review we focus on measurements relevant to the MPL. When considering the reported numbers, one should also bear in mind that in reality, PEMFC porous materials are not uniformly compressed [10].

Ex-situ *flux meter measurements*

Due to the properties of the most common PEMFC materials (compressibility and transparency) the established means of measurement has become a double piston heat flux meter that captures the actual thickness, heat flux, and the temperature drop across samples due for investigation [11]. The heat flux and temperature difference for each sample or sample stack are used to determine the thermal resistivity in a similar manner as the ohmic resistivity can be determined from an electrical flux and the corresponding potential drop. The determined thermal resistivity of the sample or the stack at this point in data reduction is actually the thermal resistivity of the sample/stack, $R_{sample/stack}$, plus the thermal contact resistivity at each end of the stack, $2R_{contact}$, see Eq. (1). The contact thermal resistivity of the contacts and the stack are then deconvoluted by plotting the total thermal resistivity as a function of the stack thickness, δ. According to Fourier's law of heat, the inverse of the slope is the thermal conductivity, see Eq. (2).

$$R_{total} = R_{sample/stack} + 2R_{contact} \quad (1)$$

$$R_{total} = \frac{1}{k}\delta + 2R_{contact} \quad (2)$$

This solution (Eqs. (1) and (2)), however, is not necessarily that straight forward. When increasing the stack thickness, one is in many instances left with the option to stack materials on top of each other in order to change the thickness. In doing so, there is an additional thermal contact resistivity introduced [12]. The sample/stack thermal resistivity is then deconvoluted into Eq. 3

$$R_{sample/stack} = nR_{sample} + (n-1)R_{sample-sample} \quad (3)$$

where n is the amount of samples, R_{sample} is the thermal resistivity of a single sample, and $R_{sample-sample}$ is the thermal contact between each sample. The challenge is then to differentiate between the two thermal resistivities, R_{sample} and $R_{sample-sample}$, because they are linearly dependent and leave a matrix with no determinant. Another way of explaining this is that adding another sample in a stack does not genuinely add a new equation to the list of unknowns. In order to deal with this problem one either needs to demonstrate that the sample–sample resistivity is negligible (which it is demonstrated to be, when stacking PTLs or MPLs) or one needs materials that come in different thicknesses so that the sample–sample resistivity is no longer present [11–13].

In the available literature, the thermal conductivity of the PTL is measured by several groups and it has been fairly safe to say that this property is becoming well understood in the scientific community. A thorough review that covers several mechanical aspects of thermal and mechanical properties of the PTL and also to some extent the MPL is given by Zamel and Li [14]. The one part that appears missing, is the understanding of the MPL/PTL thermal conductivity when in combination. More precisely; when the MPL is on top of the PTL it is actually three regions with different properties. These regions are the PTL (below), the MPL (on top), and a third region where the MPL and the PTL are merged together during the manufacturing. It is the deconvolution of the through-plane thermal conductivity of these three regions which, to our knowledge, is not yet covered or addressed in the literature.

Moreover, the existing measurements of the *ex-situ* flux meter method typically only include information of the MPL and the PTL in combination, sometimes compared with a PTL substrate. A list of relevant measurements reported in the literature are listed in Table 1. Among the first relevant measurements are those of Karimi et al. [15] and Burheim et al. [11]. Karimi reported the combined thermal conductivity of the SolviCore and a MPL to be in the range of 0.5 W K^{-1} m^{-1} at 10 bar compaction pressure [15]. Burheim et al. reported the PTL substrate and the MPL separately to be around 0.38 ± 0.08 and 0.5 ± 0.5 W K^{-1} m^{-1}, respectively [11]. Despite the large uncertainty of the last number (due to the chosen method) these numbers are comparable. In this comparison it appears likely that the SolviCore MPL increases the overall thermal conductivity when present on top of the PTL. Unsworth et al. reported the thermal conductivity of the SolviCore PTL with and without the MPL [16]. Their results showed that at around 9 bar compaction pressure the thermal conductivity of the bare PTL is 0.41–0.43 W K^{-1} m^{-1} and that the PTL with the MPL is 0.36–0.39 W K^{-1} m^{-1}. In this instance the overall thermal conductivity appears to be lowered by the presence of the MPL. It is reported experimentally and theoretically that at higher compression loads the MPL will impede the effective thermal conductivity of these materials when a MPL is on top of a PTL [16,17]. Again these results agree to some extent, taking the level of error of [11] into account. Generally, when comparing these results it appears that adding the MPL on top of a PTL does not change the effective thermal conductivity very much. This is also the situation when studying the effect of the MPL on the Sigracet PTLs, commonly known and sold under the label SGL. In a study using SGL24DA and SGL24DC, which correspond to the same PTL without and with MPL, Burheim et al. reported the thermal conductivity for up to 1000 h of artificial ageing (degradation) [3]. It was found that the dry sample thermal conductivity of these materials are literally the same, ranging 0.31–0.36 W K^{-1} m^{-1}, and also that the values do not change significantly with the ageing time.

Table 1 – Measured thermal conductivity of PTLs and MPLs using the *ex-situ* flux meter method.

Materials	k/W K^{-1} m^{-1}	$P_{comp.}$/bar	Reference
SolviCore + MPL	0.25–0.55	0.7–13.8	[15]
SolviCore only	0.25–0.45	4.5–14	[11]
MPL subtracted from a SolviCore	0.5 ± 0.5	9	[11]
SolviCore only	0.41–0.43	8–10	[16]
SolviCore + MPL	0.37–0.39	8–10	[16]
SGL24DA (no MPL)	0.33 ± 0.02	9	[3]
SGL24DC (with MPL)	0.35 ± 0.01	9	[3]
SGL10BA	0.34 ± 0.02	5	[18]
SGL10BC	0.36 ± 0.03	5	[18]
MPL only (10–25 wt% PTFE)	0.08 ± 0.02	9	[19]

Alzhazmi et al. reported the thermal conductivity for the through plane conductivity of a different series of the SGL, *i.e.* the SGL10BA and the SGL10BC [18]. At 5 bar compaction pressure they reported the thermal conductivity for the PTL substrate and the MPL coated PTL to be 0.34 ± 0.02 and 0.36 ± 0.03 W K^{-1} m^{-1}, respectively. In the light of these studies it seems justifiable to assume that the thermal conductivity of an MPL is 0.3–0.4 W K^{-1} m^{-1}, depending on the manufacturer. However, in a recent study by Burheim et al., it was shown that this is not necessarily the case [19]. When manufacturing MPLs on a thin copper film, it was shown that the thermal conductivity is as low as 0.08 ± 0.02 W K^{-1} m^{-1} around 9 bar compaction pressure. This was done for MPLs containing 10–25 wt% PTFE. Making catalyst layers, which have many similarities with the MPL, showed similar results, albeit the PTFE was replaced with Nafion® and with higher weight fractions [20]. It is from comparing the results in this paragraph that the objective of this article arises.

In-situ *temperature sensor method*

The method using heat flux and clamping pistons discussed previously is an *ex-situ* method, but there are also a few examples where the thermal conductivity is measured *in-situ* using thermocouples or temperature sensors that are sandwiched between the components in the PEMFC. Based on the measured or calculated heat and estimated thickness, the thermal conductivity is determined based on Fourier's law [21–23]. The drawback of this type of measurement is related to the lack of precision in thickness (or compression) of the measurements and also local disturbance of the local heat production (current density). An overview of thermal conductivities based on these measurements is given in Table 2.

For the *in-situ* studies the differentiation between the different layers is usually not considered [21,22]. In one study this was done, however. Thomas et al. reported that, under the assumption that the MPL is incompressible, the thermal conductivity of the SGL manufactured MPL and PTL substrate are 0.30 ± 0.03 and 0.12 ± 0.02 W K^{-1} m^{-1}, respectively. At first these values appear to disagree with those in the previous section, Section 1.2.1. These numbers are obtained by measuring the temperature drop and heat production under operation and under the assumption that the PTL substrate is compressed from an original 190 to 100 μm and that the MPL itself is entirely incompressible. These assumptions are justified based on other studies found in the literature [16]. The temperature measurements were done using temperature sensors that all were 35 μm thick. As we shall see later in this review, we argue that the relative compression of the MPL is much larger than the one of the PTL substrate and, moreover, the location of the 35 μm thick thermocouples adds further to the uncertainty of the thickness assessment. Under the condition that the thermal resistivity of the different layers are correct, we can discuss the reported thermal conductivity values in light of other results in the literature. The thermal conductivity is equal to the thickness divided by the thermal resistivity ($k_i = \Delta x_i / R_i$). From what is seen of compression of pure MPLs on a metal film substrate in the range of 10–15 bar compaction pressure, a thickness reduction of in the order 30–40% is likely (from 45 to 30 μm). This would shift the reported MPL thermal conductivity value from 0.30 to around 0.20 W K^{-1} m^{-1}. Moreover, if the thermocouple would penetrate half way into the CL and the MPL, the position of the point from where the thermal resistivity of the MPL is assumed to be recorded would drop by another 17 μm. This, in turn, would suggest the thermal conductivity of the MPL of Thomas et al. [23] to potentially be as low as 0.05 W K^{-1} m^{-1}. Assuming that the CL and the MPL compresses 40 μm on average for each side of the membrane, the thermal conductivity estimate for the PTL substrate becomes closer to 0.17 W K^{-1} m^{-1}. In this perspective the *in-situ* values are not necessarily so different from those obtained with the *ex-situ* method, though the impact of a three layer region is not at all considered in this evaluation.

Table 2 – Thermal conductivities from *in-situ* measurements.

PEMFC component type			Reference
ETEK ELAT + catalyst	k/W K^{-1} m^{-1}	0.2 ± 0.1	[21]
400 μE-TEC® + Nafion® 112	k/W K^{-1} m^{-1}	0.3–0.4	[22]
SGL 25BA	R/10^{-4} K m^2 W^{-1}	8.5 ± 0.05	[23]
SGL 25BC overall	R/10^{-4} K m^2 W^{-1}	8.74 ± 0.18	[23]
SGL 25BC subtracting the MPL contribution	k/W K^{-1} m^{-1}	0.12 ± 0.12	[23]
SGL 25BC only the MPL	k/W K^{-1} m^{-1}	0.30 ± 0.03	[23]

The laser flash method

As mentioned earlier in this section, the laser flash thermal conductivity meter method is not suited for measuring thermal conductivity of most PEMFC components. This is because most materials are compressed and contain liquid water in a real PEMFC and because many of the components are so porous that the laser is likely to flash through the samples. However, when it comes to the MPL, the pore structure is so that the MPL appears dense and solid. In an effort to asses the thermal conductivity of a MPL, Burlatsky et al. used a modified laser flash technique for a Toray PTL with a MPL (total thickness of 250 μm) on top and corrected the values to be 0.097 W K^{-1} m^{-1} for the PTL and 0.80 W K^{-1} m^{-1} for a Toray PTL paper without PTFE, see Ref. [24] and references therein. In comparison to other results, this would correspond to a Toray TGP-H-060 with a MPL of around 40 μm MPL on top of it [25,26]. The weakness with this study, however, is that since few details are known about the compaction pressure it is difficult to compare to other studies, albeit the values are similar to those seen in the rest of the study. Thus the reported values should not be considered fully trustworthy.

Aim and outline

As is seen in the literature overview on the measured thermal conductivities, there are generally two conclusions about the thermal conductivity of the MPL; it is in the order of 0.1 W K^{-1} m^{-1} when studied by means where it is treated as a single layer or it is in the order of 0.3–0.4 W K^{-1} m^{-1} when in combination with a PTL. A third option is the three region model discussed in this review.

The outline of the rest of this paper is as follows; we first present the experimental means of some of the important SGL

PTL materials including the manufacturing of a custom made MPL on a commercial SGL25BC, next an evaluation of the different regional thickness and then an evaluation of the regional thermal conductivity. Eventually, the SGLXXBC-series characteristics are compared to a custom made MPL on a SGL25BA paper to demonstrate that the overall conclusions do depend on materials.

Materials and methods

Material fabrication

Using X-ray Computer Tomography (XCT) the intrusion of a custom made MPL on a Sigracet GDL25BA was investigated [9]. A well mixed viscous ink containing deionised water (resistivity above 5 MΩ cm @ 25 °C), Triton X-100, carbon black (Vulcan® XC72R) and 60 wt% PTFE solution (DuPont™ Teflon® PTFE TE-3859), was coated onto a 25 cm by 9 cm area on the SGL 25BA using a doctor blade. The ink had a solid content of 11.9 wt% with the composition given in Table 3. The ink has a solid content of 11.9 wt%. The height of the rear slit was 100 μm and the blade moved with a speed of 7.5 mm s^{-1}. Fig. 1 shows the doctor blade setup and a freshly coated PTL.

Characterisation methods

The PTL substrates were investigated using two techniques; *i.e.* XCT and SEM. The objective was to investigate the thickness of the regions where there is PTL only, PTL-MPL composite, and MPL only.

The system used was a General Electric phoenix nanotom® with 180 kV/15 W nanofocus X-ray tube and a 2D X-ray detector with 2300 × 2300 pixels. The X-ray source was set to 50 kV and 500 μA during imaging. 1800 projections were recorded over 250 min. Each projection was obtained by averaging 3 images and a detector shift was activated to minimize circular ring artefacts. Reconstructed volumes were analysed using VGStudioMax 2.2 at the Stellenbosch University CT Scanner Facility.

A Nova NanoSEM™ electron microscope was used to locally measure different region thicknesses of SGL25BC and in-house fabricated MPL/PTL. The MPL coated PTL and a cutting blade were submerged in liquid nitrogen for 2 min and then the PTL was cut cross-sectionally (by forcing the blade from the side of the PTL where it would meet all three regions simultaneously) and mounted using a glue resin. The MPL was scanned at magnifications between 800 and 1000 times.

Table 3 – Composition of the custom made MPL.

Composition	Weight/g	$wt\%_{dry}$
Carbon	1.992	9.9
Triton X-100	3.986	–
Water	13.510	–
PTFE solution	0.664	2.0
Total	20.152	11.9

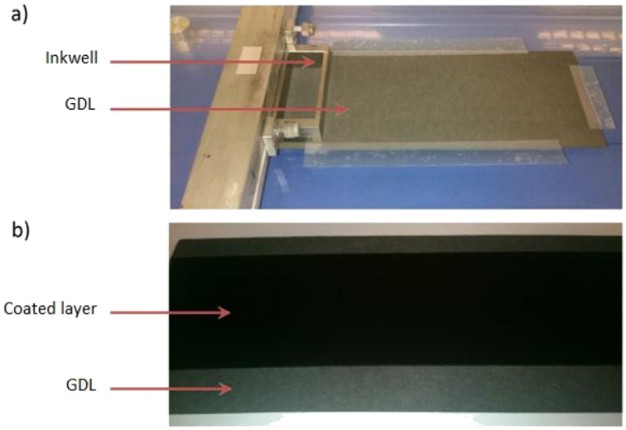

Fig. 1 – a) The doctor blade setup and b) a SGL25BA coated with the custom made MPL ink.

The thermal conductivity of the custom made MPL/PTL material is not yet reported and needed to be measured for this study. It is measured using a readily developed apparatus and procedure [3] generally described in Section 1.2.1. The measurement results and data are given in Appendix A.

Additional thermal conductivity measurements

In the instance of the custom made MPL coated SGL25BA, we also measured the thermal conductivity. This was done according to the procedure described in Section 1.2.1 and Reference [3].

Error analysis

Final reported numbers are reported with a 95% confidence interval. In some instances average values from a selection of data points are presented with the double standard deviation, 2σ, according to the selection. In other instances, the statistical distribution stems from combinations of measured and reported numbers. When combining several measured values, each with a distinct variance, σ, the new variance is calculated from the propagation of error function, Eq. (4).

$$\sigma_i^2 = \sum_{n=1}^{i} \left(\frac{\partial f(x_1, x_2, \ldots, x_i)}{\partial x_n} \sigma_n \right)^2 \quad (4)$$

where f is a function of several variables, $x_{1,2,3,etc.}$, each with their own standard deviation, $\sigma_{x_{1,2,3,etc.}}$.

Results and discussion

In this study, the SGL BA-series is the denominator and we either look at the commercial MPL on the SGL BC-series (BA with MPL) or our own MPL made on top of an SGL BA-series. We first investigate the thickness of the subregions of these materials and next the deconvoluted thermal conductivities.

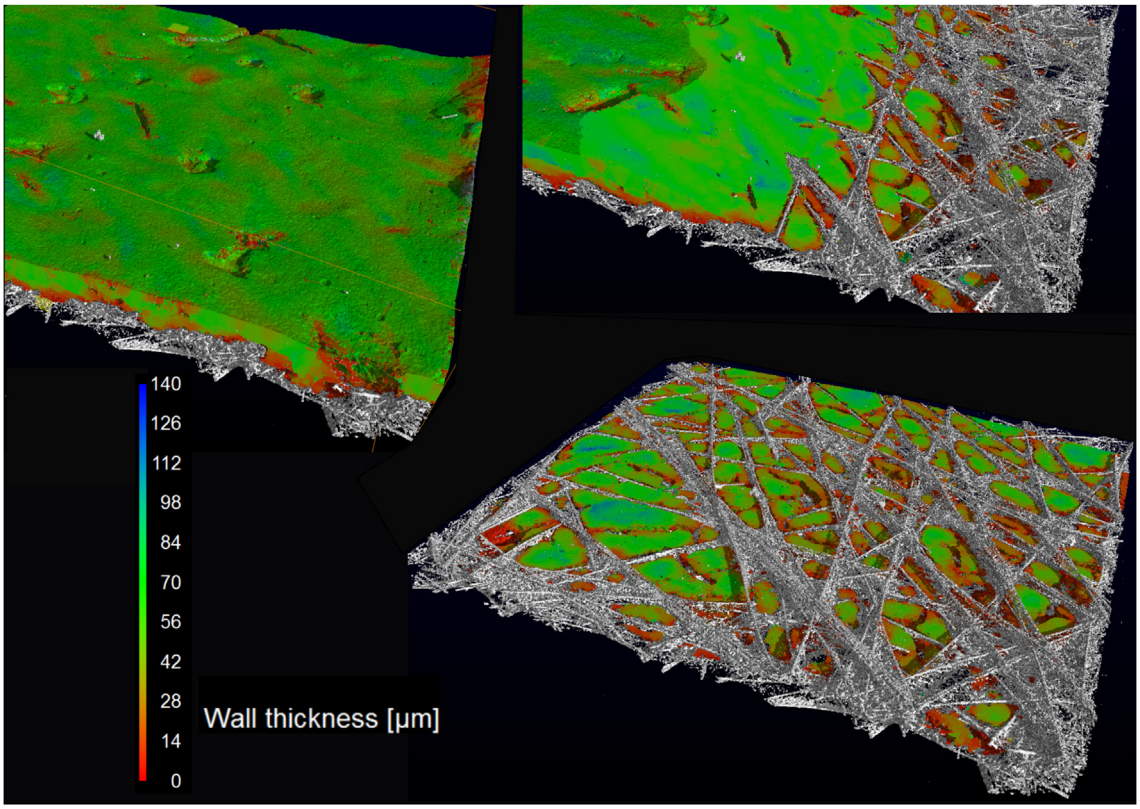

Fig. 2 – XCT depictions of a SGL25BC showing 3D-depictions of the MPL (coloured based on layer thickness) and the PTL substrate (grey).

Thickness evaluation

The SGL BC-series

The SGL24BC XCT 3D scans are depicted in Fig. 2. This figure shows the thickness of the MPL material by the colours according to the thickness scale and the PTL fibres in a grey tone. The software tools allows for the MPL to be removed separately from the PTL in the graphical representation. This is done in two ways in Fig. 2: First a ~20° plane is used to remove the MPL (upper right) so that one can see how the MPL is present as one looks deeper into the PTL (SGL24BA) region, and second (lower right) everything above the start of the interface is removed. By looking at the colours of the intruded MPL in this latter picture one can also see to what extent the MPL body spreads out inside the PTL. One can thus see that the MPL and the PTL forms a composite region constituting of the MPL as the matrix and the PTL fibres as fibres.

In Fig. 3 we have investigated the MPL and the nearest region with the MPL of a SGL35BC. The SGL35xx hold many similarities to the SGL24xx and SGL25xx. It is much thicker, but the porosity is in between the 24 and 25-series while at the same time it has the same MPL-on-top-thickness (or at least the given thickness differences indicate this in the published data sheet) [27]. Since we in this study compare different studies including the SGL-24/25-BA/BC samples, the SGL35BC is a good choice for comparing the MPL and its intrusion between the SGL-24/25-BC samples due to the SGL35-substrate intermediate porosity. In Fig. 3 the thickness of the MPL-on-top and the MPL-intrusion are indicated by faded white stripes and white dots, respectively. For the picture indicated A, the MPL was carefully removed before freezing, cutting and mounting. For the micrographs indicated B-D, the MPL was mounted as is (after freeze cutting) and these were used to asses and measure the thickness of the MPL-on-top and MPL-intrusion regions. The obtained thickness values are presented in Table 4. The thickness of the MPL-on-top vary from as thin as 23 μm up to 43 μm. The MPL-intrusion thickness varies from 29 to 49 μm. For both of these the range of thickness represents a doubling of the lower value. When evaluating the total thickness of the two together the trend is that when the MPL-on-top is thin the MPL-intrusion is thick and *vice versa*. This can be seen from the numbers in Table 4. The mean thickness of the sum of the two layers is 74 ± 15 μm and the two layers are individually 33 ± 14 and 41 ± 15 μm. If the thickness of these regions were not correlated as just explained, the error of propagation (see Eq. (4)) should lead to a mean thickness of the sum of the two to be 74 ± 21 rather than 74 ± 15 μm. That is, the error of propagation formula, Eq. (4), maximises errors by treating every single standard deviation as an independent stochastic variable. The averaging method of the single sums (row three in Table 4), on the other hand, gives a confidence interval based on systematic changes and relations. Therefore, when the averaging approach suggests a smaller confidence interval than the error of propagation formula does, there is statistical support for the claim that the sum of the MPL-on-top- and MPL-intrusion-thickness is

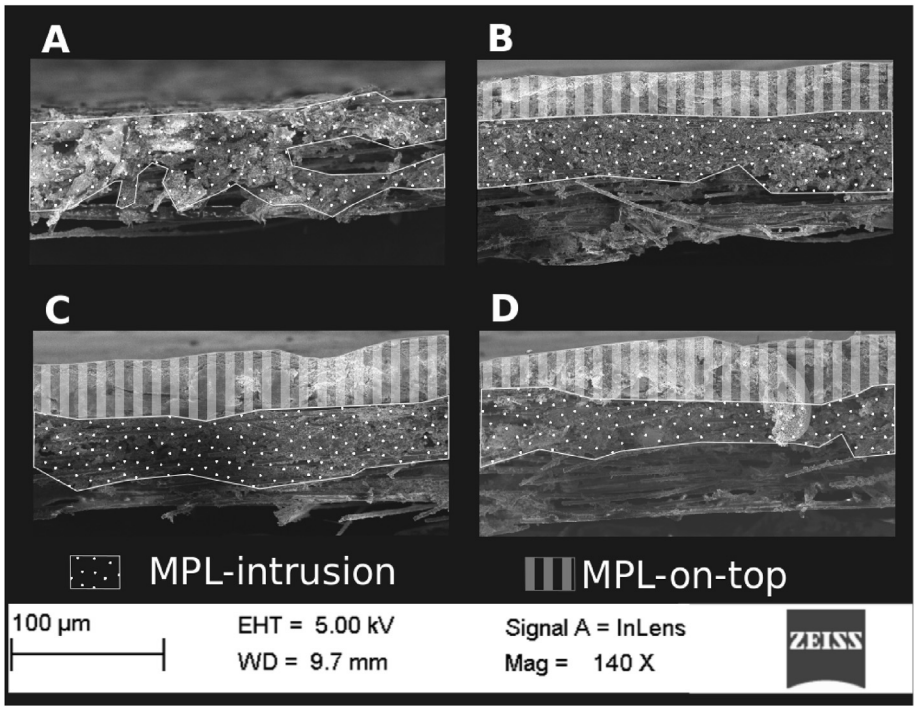

Fig. 3 – The MPL-PTL interface for a SGL35BC with the MPL-on-top and MPL-intrusion regions indicated. A: The MPL-on top region is removed. B–D: Uncompressed SGL35BC.

somewhat constant. The local thinning of the MPL-on-top can simply be due to the SGLxxBA having a local increase in thickness (a bump sticking out) and a local thickening could be due to a surface hole in the top of the SGLxxBA making the MPL-on-top becoming thinner. Since the total thickness is fairly constant, it means that the bump would lead to the same intrusion depth except that locally it appears more and with a hole the intrusion would appear locally smaller, although it only appears this way. The fact that a local change in thickness for the MPL-on-top is somewhat compensated by a change in the MPL-intrusion thickness is important when evaluating both the local and overall thermal conductivity. We shall return to this point when evaluating the thermal conductivities in Section 3.2.

Custom made MPL on the SGL25BA

Due to the low viscosity of the coated ink, it was found that the majority of the custom made MPL intruded into the SGL25BA substrate. An XCT depiction of the composite region of the PTL fibres with the MPL as a matrix is shown in Fig. 4 (left). To the right in this figure, a SEM micrograph including the MPL-on-top thickness indication is given. The suggested thickness is up to 20 μm, which is twice the thickness of the fibres. When investigating cuts made on several different locations it was in many places difficult to assess the MPL-on-top thickness. Moreover, when measuring the thickness of the uncompressed materials the recorded thickness was found to be 194 ± 19 μm. This thickness is the reported thickness of the SGL24/25BA materials [28].

When it comes to the MPL-intrusion thickness of the custom made MPL, the MPL appeared scattered throughout the PTL substrate. This can be seen in Fig. 4 and is representative for the investigation in several other locations of the material. Since the custom made MPL material has a different distribution than the commercial one it can be difficult to differentiate the thermal conductivity regions in the same manner as we do with the commercial one. However it is still relevant to compare a material with three distinct regions to a material with only one.

Thermal conductivity analysis

In Table 5, all the thickness data relevant for the thermal conductivity comparison is summarised. This constitutes of

Table 4 – Thickness measurements of the MPL-on-top and MPL-intrusion thickness for the SGL35BC.

Region thickness															Mean
$\delta_{MPL-on-top}/\mu m$	23	26	29	31	31	40	34	31	43	20	34	43	40	34	33 ± 14
$\delta_{MPLintrusion}/\mu m$	43	40	43	34	54	49	37	49	40	51	40	29	29	40	41 ± 15
$\sum_{MPL-on-top}^{MPL-intrusion} \delta_i/\mu m$	66	66	71	66	86	89	71	80	83	71	74	71	69	74	74 ± 15

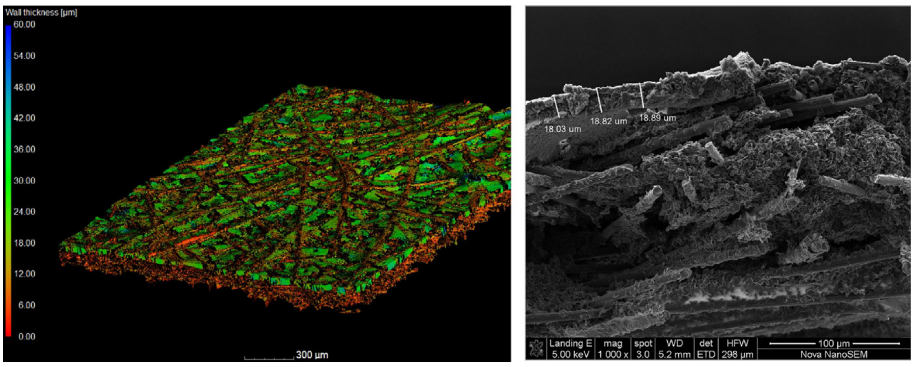

Fig. 4 – Left: XCT 3D visualisation of the SGL25BA with the custom made MPL on top. Right: SEM micrograph indicating thicknesses of the MPL on top of the SGL25BA substrate. One can see that the majority of the MPL is deposited inside the SGL25BA substrate.

the SGL24/25 BA (no MPL), the SGL 24/25 BC (commercial MPL), the difference between these two (the commercial MPL-on-top), a custom made MPL on copper, and the present custom made MPL on a SGL25BA - all at almost no or 9.3 bar compaction pressure. The tabulated data summarises measurements from manufacturing data sheets [28], measurements previously reported [3,13,19], and measurements that are new in this study. In essence, MPLs are compressed to 30–60% of the uncompressed thickness while the SGL PTL substrate is only compressed to 80–90% of the pristine thickness. This is important to take note of before we progress in this analysis. What we see here, is that when compressing a PTL with a MPL, the on-top-MPL will be compressed to 30–60% while the MPL integrated in the PTL will be compressed to the same degree as the PTL itself, *i.e.* 80–90%.

Regarding the SGL24BC, it is clear from the XCT (Fig. 2) and the SEM (Fig. 3) figures that the material has three distinct regions; PTL, MPL-PTL composite, and MPL. When it comes to the custom made MPL on the SGL25BA, this material appears to have a distribution that is more randomly distributed inside the PTL, with a continuous matrix region on the entrance side and a gradual thinning as one looks closer to the other side. In comparison to the commercial MPL (of the SGL24BC), the custom made on the SGL25BA appears much less dense and less continuous. This can be related to the manufacturing procedure. For instance, if the custom made MPL has a very low viscosity, it will sink more into the MPL than if it has higher viscosity. In fact, for the larger study that the custom MPL was originally made for, a more viscous MPL ink was also made and the result was a more dense MPL that formed a more distinct distribution inside the MPL and also a separate layer on top - much more like the commercial MPL of the SGL24/BC. These are effects (MPL distribution and ink viscosity) that are very important when comparing the thermal conductivity values.

Returning the focus to the SGL24BC and the different regions, the thermal resistivity of this layer is the sum of the resistivity of each layer, Eq. (5). The relation between the thickness, thermal conductivity, and thermal resistivity of each of these regions follows accordingly, Eq. (6). From this, in turn, the thermal conductivity of the MPL-PTL composite region can be determined, Eq. (7). Table 6 gives an overview of the values relevant for this analysis. In addition (to the very right), the thermal conductivity, thickness, and thermal resistivity of the presently custom made MPL integrated with the SGL24BA is given as well. Here, they serve as a reference to illustrate that the subject of discussion is not always as straight forward as it appears at first with the SGLxxBC series.

$$R_{tot} = R_{PTL} + R_{composite} + R_{MPL} \tag{5}$$

$$\frac{\delta_{tot}}{k_{tot}} = \frac{\delta_{PTL}}{k_{PTL}} + \frac{\delta_{comp.}}{k_{comp.}} + \frac{\delta_{MPL}}{k_{MPL}} \tag{6}$$

$$k_{comp.} = \frac{\delta_{comp.}}{\left(\frac{\delta_{tot}}{k_{tot}} - \frac{\delta_{PTL}}{k_{PTL}} - \frac{\delta_{MPL}}{k_{MPL}}\right)} = \frac{\delta_{comp.}}{(R_{tot} - R_{PTL} - R_{MPL})} \tag{7}$$

Discussion

Using the results found this far in combination with literature values, we have assessed reasonable thickness, thermal conductivity, and thermal resistivity values of the material regions to proceed the deconvolution of the thermal conductivity of the MPL-PTL composite region of the commercial material.

Table 5 – Survey of thickness at different pressures. From left: the SGL 24 and 25, with and without the Sigracet MPL (BA and BC), the subtracted SGL-MPL, single MPLs and the custom made MPL on top of the SGL25BA. Values given refer to compression at 9 bar relative to uncompressed [3,19,28].

	P/bar	SGL24BA & SGL25BA	SGL24BC & SGL 25BC	On-top-MPL BC-BA	MPL on copper	Present MPL on SGL25BA
δ/µm	≤0.24	190 [28]	235 [28]	45	60 [19]	194 ± 19
δ/µm	9.3	174 ± 5 [3]	190 ± 2 [3]	16 ± 5	32 ± 5 [19]	158 ± 8
Compr./%	–	92 ± 3	82 ± 1	36 ± 20	53 ± 9	81 ± 8

Table 6 – Evaluation of thickness of the different regions of SGL24/25BC and the custom coated MPL.

	P/bar	SGL24/25 no MPL	SGL-MPL composite	MPL on top	SGL24/25BC total	SGL25BA + present MPL
δ/μm	≤0.24	117 ± 33	70 ± 30	36 ± 19	226 ± 19	194 ± 19
δ/μm	9.3	107 ± 30	67 ± 30	19 ± 11	193 ± 12	158 ± 8
$R/10^{-4}$ K m^2 W^{-1}	9.3	3.2 ± 0.9	**−0.09 ± 1.8**	2.4 ± 1.5	5.5 ± 0.4	5.1 ± 1.7
k/W K^{-1} m^{-1}	9.3	0.33 ± 0.02	**0 ± 150**	0.08 ± 0.02	0.35 ± 0.01	0.318 ± 0.012

When comparing the total thermal resistivity of a MPL coated PTL, one can see that the thermal resistivity, R, of the PTL-only region (3rd column) and the MPL-on-PTL region (5th column) in combination is equivalent to the one of the entire assembly (6th column). (There are in total 7 columns.) This means that when rearranging Eq. (5) to obtain the thermal resistivity of the SGL-MPL-composite region one is not only left with a very small number, one is actually left with a negative one. Moreover, and mainly due to variations in thickness and a small difference, one is left with a rather large uncertainty. It is then very difficult to asses the thermal conductivity of the SGL-MPL-composite region, albeit we realise that this region is the one with the highest thermal conductivity among the PEMFC components. This means that cross sectional temperature differences would consist of three gradients; a steep one in the MPL region on top of the PTL/MPL-PTL-composite region, an almost flat one in the MPL-PTL-composite region, and an intermediate in the region where there is only PTL. This qualitative relation between cross sectional thermal gradients would be valid regardless of whether or not water is present in the sole PTL region.

The composite region obviously has much better thermal conductivity than the two other regions assembling the MPL coated PTL. Perhaps it appears contradictory that two materials with low thermal conductivity (PTL-only and MPL-only) comprise a material with very high thermal conductivity (MPL-PTL-composite). This must then be seen in the light of other similar materials. For instance, graphitized carbon fibres are used as a matrix for a polymer in a concept also known as polymer composite heat exchangers [29]. When making a polymer composite heat exchanger where the fibres were aligned in-plane, the overall thermal conductivity was 1.0 ± 0.3 W K^{-1} m^{-1}, although the thermal conductivity of a polymer is typically in the range of 0.10–0.30 W K^{-1} m^{-1} [30]. Applying these data (thermal conductivity of 1.0 ± 0.3 W K^{-1} m^{-1}) to this analysis would result in a thermal resistivity of the MPL-PTL-composite layer equivalent to 0.7 ± 0.4 10^{-4} K m^2 W^{-1}. Thus we have a region consisting of two materials that individually have poor thermal conductivity, but that together comprise a material with very high thermal conductivity. As seen in this study, care should be taken regarding this assumption as not all MPLs have as distinguished distribution in the PTL substrate as is the case with the SGL24/25BC.

Conclusion

Using X-ray computer tomography and scanning electron microscopy, it was possible to study the interfacial region of a micro porous layer (MPL) and a porous transport layer (PTL), in this case the SGL24/25/35-series. It was found that the MPL would intrude the PTL to form a composite region that could take up as much as a third of the PTL thickness. Thus the MPL coated PTL consists of three regions; a PTL-only region, a MPL-PTL-composite region, and a MPL-only region.

Accounting for literature values for thermal conductivities and compression values of the materials relevant in this study, it can be concluded that the MPL-PTL-composite region conducts heat far better than the other materials and the MPL-only region conducts heat the least. For the commercial GDL, the region where the MPL intrudes the GDL has the highest through-plane thermal conductivity this region thickness should be enlarged and the pure MPL region thickness lowered in order to give the PEMFC a more uniform temperature distribution. Generally, it can be concluded that with respect to PEMFC cooling, the MPL-only region should be as thin as possible. Investigating other materials with more randomly distributed MPLs gave different results.

Acknowledgments

ENERSENSE is acknowledged for financial support.

A. Thermal conductivity of the custom made MPL

The thermal conductivity of a micro porous layer with 11.9 w% MPL on SGL25BC was investigated. Four circular samples with a diameter of 0.021 m were punched out of one sheet of this carbon paper. These samples were then subsequently measured in the thermal conductivity device at a compaction pressure of 9.3 bar. To investigate the thermal conductivity the heat flux was measured for one sample first, then for two samples on top of each other, then for three and finally for four samples on top of each other. While stacking, the samples were aligned in such a manner that same surfaces, either coated or uncoated, came into contact with each other. The sample sample thermal contact resistance is negligible, according to Burheim et al. [3]. The thickness of the sample stack was

Table 7 – Measured thickness and thermal resistivity for the SGL24BA coated with the custom made MPL.

Measurement number	Stack thickness /10^{-6} m	Added thickness /10^{-6} m	Therm. resist. /10^{-4} K m^2 W^{-1}
1	163	163	8.4
2	320	157	15.1
3	473	153	18.8
4	630	158	24.0
Mean	–	158 ± 8	

recorded for every stack, see Table 7. The choice of measuring the samples by adding one sample for every measurement point rather than adding a stack of pristine samples was made due to the scarcity of material samples. Likewise to a previous study [3], this study includes materials originally prepared for another study [9]. In many studies, thermal conductivity investigation is not originally included, and as a consequence the option of preparing samples to also cover the thermal conductivity measurement procedure is neglected and (like in the present study) one is left with material scarcity. A thermal resistance was obtained for every sample stack, see Table 7. The inverse of the gradient of thermal resistance with thickness is the thermal conductivity, see Ref. [3]. Thus the slope of a linear regression of the obtained thermal resistance results is the average thermal conductivity of all sample stacks, see Fig. 5. The thermal conductivity for the investigated material was found to be $0.308 \pm 0.012\ W\ K^{-1}\ m^{-1}$. The thermal conductivity apparatus was calibrated using materials with known thermal conductivity, see Ref. [11]. These values are known with 5% accuracy and thus this is the accuracy limitation of the reported values in this paper.

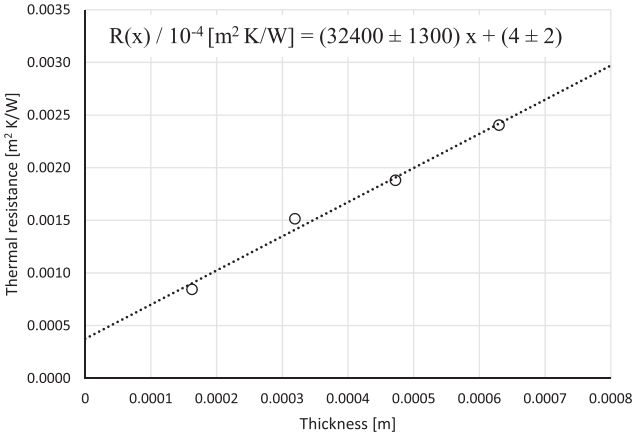

Fig. 5 – Measured specific thermal resistivity as a function of thickness at 9.3 bar compaction pressure.

B. Additional remark

Since submitting this manuscript, Andisheh-Tadbir et al. submitted and published a study comparing thermal resistivity of SGL 24BA, 24BC, 34BA, and 34 BC [31]. By subtraction of thermal resistances of the different materials and comparing difference in thickness, they estimated the thermal conductivity of the MPL on top to be in the range of $0.1–0.2\ W\ K^{-1}\ m^{-1}$ for a compaction pressure range of 1–6 bar [31]. The study by Andisheh-Tadbir et al. did not account for the third region where the MPL is integrated into the PTL region. Based on the analysis in the present paper, their suggested values would lower by in the order of a factor of two and fit to the values reported in Ref. [19].

REFERENCES

[1] de Bruijn F, Dam VAT, Janssen G. Review: durability and degradation issues of PEM fuel cell components. Fuel Cells 2008;08:1–22.
[2] Yuan X, Li H, Zhang S, Martin J, Wang H. A review of polymer electrolyte membrane fuel cell durability test protocols. J Power Sources 2011;196:9107–16.
[3] Burheim OS, Ellila G, Fairweather JD, Labouriau A, Kjelstrup S, Pharoah JG. Ageing and thermal conductivity of porous transport layers used for pem fuel cells. J Power Sources 2013;221:356–65.
[4] Seland F, Berning T, Børresen B, Tunold R. Improving the performance of high-temperature PEM fuel cells based on PBI electrolyte. J Power Sources 2006;160:27–36.
[5] Qi Z, Kaufman A. Improvement of water management by a microporous sublayer for pem fuel cells. J Power Sources 2002;109:38–46.
[6] Gostick JT, Ioannidis MA, Fowler MW, Pritzker MD. On the role of the microporous layer in PEMFC operation. Electrochem Commun 2009;11(3):576–9.
[7] Lee J, Hinebaugh J, Bazylak A. Synchrotron x-ray radiographic investigations of liquid water transport behavior in a PEMFC with MPL-coated GDLs. J Power Sources 2013;227:123–30.
[8] Deevanhxay P, Sasabe T, Tsushima S, Hirai S. Effect of liquid water distribution in gas diffusion media with and without microporous layer on PEM fuel cell performance. Electrochem Commun 2013;34:239–41.
[9] Crymble GA. Towards reliable correlation of microporous layer physical characteristics and pemfc electrochemical performance [Master's thesis]. University of Cape Town; November 2014.
[10] Millichamp J, Mason TJ, Neville TP, Rajalakshmi N, Jervis R, Shearing PR, et al. Mechanisms and effects of mechanical compression and dimensional change in polymer electrolyte fuel cells – a review. J Power Sources 2015;284:305–20.
[11] Burheim O, Vie P, Pharoah J, Kjelstrup S. *Ex-situ* measurements of through-plane thermal conductivities in a polymer electrolyte fuel cell. J Power Sources 2010;195:249–56.
[12] Ramousse J, Lottin O, Didierjean S, Maillet D. Estimation of the thermal conductivity of carbon felts used as PEMFC gas diffusion layers. Int J Therm Sci 2008;47:1–6.
[13] Burheim OS, Aslan M, Atchison JS, Presser V. Thermal conductivity and temperature profiles in carbon electrodes for supercapacitors. J Power Sources 2014;246:160–6.
[14] Zamel N, Li X. Effective transport properties for polymer electrolyte membrane fuel cells – with a focus on the gas diffusion layer. Prog Energy Combust Sci 2013;39:146.
[15] Karimi G, Li X, Teertstra P. Measurement of through-plane effective thermal conductivity and contact resistance in {PEM} fuel cell diffusion media. Electrochim Acta 2010;55:1619–25.
[16] Unsworth G, Zamel N, Li X. Through-plane thermal conductivity of the microporous layer in a polymer electrolyte membrane fuel cell. Int J Hydrogen Energy 2012;37:5161–9.
[17] Zamel N, Becker J, Wiegmann A. Estimating the thermal conductivity and diffusion coefficient of the microporous layer of polymer electrolyte membrane fuel cells. J Power Sources 2012;207:70–80.
[18] Alhazmi N, Ingham D, Ismail M, Hughes K, Ma L, Pourkashanian M. The through-plane thermal conductivity and the contact resistance of the components of the membrane electrode assembly and gas diffusion layer in proton exchange membrane fuel cells. J Power Sources 2014;270:59–67.
[19] Burheim OS, Su H, Pasupathi S, Pharoah JG, Pollet BG. Thermal conductivity and temperature profiles of the micro

porous layers used for the polymer electrolyte membrane fuel cell. Int J Hydrogen Energy 2013;38:8437–47.
[20] Burheim OS, Su H, Hauge HH, Pasupathi S, Pollet BG. Study of thermal conductivity of pem fuel cell catalyst layers. Int J Hydrogen Energy 2014:9397–408.
[21] Vie P, Kjelstrup S. Thermal conductivities from temperature profiles in the polymer electrolyte fuel cell. Electrochim Acta 2004;49:1069–77.
[22] He S, Mench MM, Tadigadapa S. Thin film temperature sensor for real-time measurement of electrolyte temperature in a polymer electrolyte fuel cell. Sensors Actuat A Phys 2006;125(2):170–7.
[23] Thomas A, Maranzana G, Didierjean S, Dillet J, Lottin O. Thermal and water transfer in pemfcs: investigating the role of the microporuos layer. Int J Hydrogen Energy 2014;39:2649–58.
[24] Burlatsky SF, Atrazhev VV, Gummalla M, Condit DA, Liu F. The impact of thermal conductivity and diffusion rates on water vapor transport through gas diffusion layers. J Power Sources 2009;190:485–92.
[25] Khandelwal M, Mench MM. Direct measurement of through-plane thermal conductivity and contact resistance in fuel cell materials. J Power Sources 2006;161:1106–15.
[26] Burheim O, Lampert H, Pharoah J, Vie P, Kjelstrup S. Through-plane thermal conductivity of PEMFC porous transport layers. J Fuel Cell Sci Technol 2011;8. 021013-1–11.
[27] S. GROUP, SIGRACET GDL, gas diffusion layer 2D non-woven fabric. November 2014. http://www.sglgroup.com/cms/_common/downloads/products/product-groups/su/fuel-cell-components/SIGRACET_GDL_2D_TDS-TI.RS.033.pdf.
[28] S. GROUP, SIGRACET, GDL 24 & 25 series gas diffusion layer. November 2014. www.ion-power.com/res/Sigracet/GDL_24_25_Series_07.pdf.
[29] Robinson F, Cevallos JG, Bar-Cohen A, Bruck H. Modeling and validation of a prototype thermally-enhanced polymer heat exchanger. ASME 2011 Int Mech Engin Expo IMECE2011-65684 2011:1–10.
[30] West RC. CRC – handbook of physical and chemical properties. 58th ed. CRC Press, Inc.; 1977-1978.
[31] Andisheh-Tadbir Mehdi, Kjeangm Erik, Bahrami Majid. Thermal conductivity of microporous layers: Analytical modeling and experimental validation. J Power Sources 2015;296:344–51. http://dx.doi.org/10.1016/j.jpowsour.2015.07.054.